



Originally published as:

Lu, C., Li, X., Ge, M., Heinkelmann, R., Nilsson, T., Soja, B., Dick, G., Schuh, H. (2016): Estimation and evaluation of real-time precipitable water vapor from GLONASS and GPS. - *GPS Solutions*, 20, 4, pp. 703–713.

DOI: <http://doi.org/10.1007/s10291-015-0479-8>

Estimation and evaluation of real-time precipitable water vapor from GLONASS and GPS

Cuixian Lu¹, Xingxing Li¹, Maorong Ge¹, Robert Heinkelmann¹, Tobias Nilsson¹, Benedikt Soja¹, Galina Dick¹ and Harald Schuh¹

1. German Research Centre for Geosciences GFZ, Telegrafenberg, 14473 Potsdam, Germany

Abstract: The revitalized Russian GLONASS system provides new potential for real-time retrieval of zenith tropospheric delays (ZTD) and precipitable water vapor (PWV) in order to support time-critical meteorological applications such as nowcasting or severe weather event monitoring. In this study, we develop a method of real-time ZTD/PWV retrieval based on GLONASS and/or GPS observations. The performance of ZTD and PWV derived from GLONASS data using real-time precise point positioning (PPP) technique is carefully investigated and evaluated. The potential of combining GLONASS and GPS data for ZTD/PWV retrieving is assessed as well. The GLONASS and GPS observations of about half a year for 80 globally distributed stations from the IGS (International GNSS Service) network are processed. The results show that the real-time GLONASS ZTD series agree quite well with the GPS ZTD series in general: the RMS of ZTD differences are about 8 mm (about 1.2 mm in PWV). Furthermore, for an inter-technique validation, the real-time ZTD estimated from GLONASS-only, GPS-only, and the GPS/GLONASS combined solutions are compared with those derived from Very Long Baseline Interferometry (VLBI) at co-located

GNSS/VLBI stations. The comparison shows that GLONASS can contribute to real-time meteorological applications, with almost the same accuracy as GPS. More accurate and reliable water vapor values, about 1.5-2.3 mm in PWV, can be achieved when GLONASS observations are combined with the GPS ones in the real-time PPP data processing. The comparison with radiosonde data further confirms the performance of GLONASS-derived real-time PWV and the benefit of adding GLONASS to stand-alone GPS processing.

Keywords: GLONASS; zenith tropospheric delay; precipitable water vapor; real-time precise point positioning; VLBI; radiosonde

Introduction

The potential of GPS observations for troposphere monitoring was first described in Bevis et al. (1992) concerning post-processing solutions. The near real-time (NRT) tropospheric solutions, which are suitable for numerical weather prediction (NWP) models, were then developed and evaluated by extensive investigations (Rocken et al. 1997; Gendt et al. 2001; Elgered et al. 2005). Several projects such as WAVEFRONT, MAGIC, and European Cooperation in Science and Technology (COST-716), have demonstrated the ability of GPS serving as an accurate water vapor sensor for meteorological and climatological applications (Haan et al. 2004; Gutman et al. 2004; Nilsson and Elgered 2008). As a notable example, within the European E-GVAP (<http://egvap.dmi.dk>) project, a ground tracking network consisting of more than 2400 continuously operating GPS stations is deployed to provide NRT PWV (precipitable water vapor) estimates for assimilation into NWP models.

To fully exploit the potential of GNSS (Global Navigation Satellite Systems) for real-time monitoring and forecasting of severe weather events, the development and transition from the NRT mode to the true real-time mode of tropospheric monitoring has become one of the current topics, such as for the new European COST Action ES1206 (http://www.cost.eu/COST_Actions/essem/Actions/ES1206). During recent years the International GNSS Service (IGS) has coordinated the development of global real-time orbit and clock products, exploiting individual contributions from several institutions in order to guarantee its high robustness and availability. At the end of 2012, the IGS launched its Real-Time Service (RTS, [Caissy et al. 2012](#)) and declared the product as official. Thanks to these developments, precise point positioning (PPP, [Zumberge et al. 1997](#)) has been successfully applied for real-time water vapor retrieving and for supporting time-critical meteorological applications, such as NWP nowcasting or severe weather event monitoring ([Li et al. 2014](#); [Dousa and Vaclavovic 2014](#); [Yuan et al. 2014](#); [Shi et al. 2015](#)).

The Russian GLObal NAVigation Satellite System (GLONASS) has been revitalized and is now fully operational with 24 satellites in orbit (<http://www.glonass-ianc.rsa.ru/en/GLONASS/>). It has been going through gradual modernization and the FDMA (Frequency Division Multiple Access) mode is scheduled to change to CDMA (Code Division Multiple Access) mode, which is consistent with other GNSS systems concerning the convenience for integer ambiguity resolution ([Cai and Gao 2013](#)). At present, more than 200 stations operated by IGS can continuously provide both GPS and GLONASS observations. Consequently, several investigations focusing on adding GLONASS satellites to GPS for precise positioning have been carried out, and results

demonstrate that the combined GPS/GLONASS PPP solution is more accurate and more robust than the GPS-only solution in terms of positioning, with significantly reduced time for position convergence ([Cai and Gao 2013](#); [Li et al. 2015](#)).

However, so far only limited studies related to using GLONASS data only or in combination with GPS data for tropospheric parameter estimation have been conducted. Bruyninx ([2007](#)) pointed out an underestimation of about 0-2 mm in ZTD (zenith total delays) estimates from the combined GPS and GLONASS PPP solution compared to the GPS-only solution. A systematic bias between the ZTD derived from GPS and GLONASS in NRT solution was identified by Dousa ([2010](#)), with the GLONASS ZTD resulting in approximately 1-3 mm lower values compared to those estimated from GPS using a network of 38 European stations. Furthermore, no significant improvement of the ZTD quality was found when comparing a stand-alone GPS solution with respect to the combined GPS/GLONASS solution in NRT processing. However, the initial inconsistency between stand-alone GPS and GLONASS ZTD solutions disappeared when the IGS08 antenna phase center models were adopted ([Dach et al. 2011](#)).

With the completion of GLONASS, the quality of ZTD/PWV retrieved from GLONASS data is expected to improve and increase the benefit of combining GLONASS and GPS for ZTD/PWV estimation, especially in real-time processing. We investigate the real-time ZTD/PWV retrieval from stand-alone GLONASS, GPS, and GLONASS+GPS observations based on the PPP technique. The observations of 80 globally distributed stations from the IGS network are processed in real-time PPP mode to derive three different solutions: GLONASS-only, GPS-only, and GPS/GLONASS combined solution. First, the performance

of the GLONASS-derived ZTD is assessed by comparing to those derived from GPS. All the three solutions are then compared to results derived from Very Long Baseline Interferometry (VLBI) and radiosondes (RS) to independently evaluate the performance of the GLONASS-only solution and the benefit of adding GLONASS to GPS for ZTD/PWV retrieval.

GNSS data collection and processing

The collection of data sets of GLONASS and GPS is described in this part. The observation modeling and processing strategies for real-time GNSS ZTD/PWV retrieval is also presented in details.

GNSS data collection

The IGS collects, archives, and freely distributes GNSS observation data sets from a cooperatively operated global network of several hundreds of ground tracking stations. Apart from supporting tracking of GPS, the majority of its stations are capable of providing GLONASS observations ([Dow et al. 2009](#)) as well. In this study, the GPS and GLONASS observations of about 80 stations from the IGS network are processed in simulated real-time mode. The distribution of the selected IGS stations, that can track both GPS and GLONASS satellites, is shown in Figure 1.

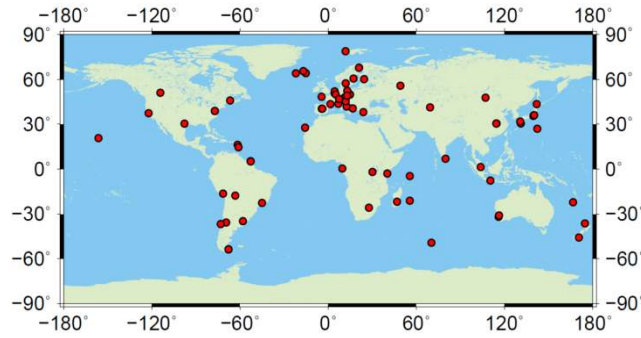


Figure 1 Distribution of the selected GPS/GLONASS IGS stations.

Real-time ZTD/PWV estimation

Generally, the ionospheric-free combination of dual-frequency carrier phase and pseudorange (LC, PC) are utilized in PPP processing to eliminate the first-order effects of the ionosphere.

The observation equations can be expressed as (Kouba 2009),

$$L = \rho + c(dt - dT) + T + \lambda N + \varepsilon_L \quad (1)$$

$$P = \rho + c(dt - dT) + T + \varepsilon_P \quad (2)$$

where L and P are the ionospheric-free combinations of carrier phase and pseudorange, ρ is the geometric distance, dt and dT denote the receiver and clock biases, c is the speed of light in vacuum, T is the tropospheric delay, λ is the wavelength, N is the unknown phase ambiguity, and ε_L and ε_P denote the measurement noise and multipath error for carrier phase and pseudorange, respectively. The first-order ionospheric delay is eliminated by the ionospheric-free linear combination, the phase center offset and variation, phase wind-up, tidal loading, earth rotation, and relativistic effects can be corrected according to existing models (Kouba 2009). In the GPS/GLONASS combined data processing, different hardware delay biases that exist in the receiving channels (Wanninger 2011) must be taken into account,

and the combined observation model can be expressed as,

$$\begin{cases} L^G = \rho^G + c(dt - dT^G) + T^G + \lambda^G N^G + \varepsilon_L^G \\ L^{R_k} = \rho^R + c(dt - dT^R) + B_L^{R_k-G} + T^R + \lambda^{R_k} N^R + \varepsilon_L^R \end{cases} \quad (3)$$

$$\begin{cases} P^G = \rho^G + c(dt - dT^G) + T^G + \varepsilon_p^G \\ P^{R_k} = \rho^R + c(dt - dT^R) + B_p^{R_k-G} + T^R + \varepsilon_p^R \end{cases} \quad (4)$$

where the indices G and R_k refer to the GPS and GLONASS satellite system, respectively, k denotes the frequency factor for GLONASS satellite as it uses FDMA signals, the terms $B_L^{R_k-G}$ and $B_p^{R_k-G}$ denote the receiver internal bias between GLONASS and GPS for carrier phase and pseudorange, respectively. For the GLONASS satellites with different frequency factors, the receiver internal biases $B_p^{R_k-G}$ are different and their differences are usually called inter-frequency biases (IFB). We set up the code bias parameters for each GLONASS frequency, and the code bias for GPS satellites is set to zero in order to eliminate the singularity between receiver clock and code bias parameters (Dach et al. 2006). Consequently, the estimated biases of GLONASS are relative to the biases for GPS satellites. It is worthwhile to note that such a receiver internal bias is only relevant for processing the code data, while the corresponding phase ambiguity parameters will absorb the phase delays when analyzing the phase measurements.

The slant total delay T can be modeled by hydrostatic and non-hydrostatic/wet components, which can both be expressed by their individual zenith delays and the corresponding mapping functions, and by the gradient part (Chen and Herring, 1997),

$$T = mf_h \cdot ZHD + mf_{nh} \cdot ZWD + mf_G \cdot (G_{ns} \cdot \cos(a) + G_{ew} \cdot \sin(a)) \quad (5)$$

where mf_h and mf_{nh} are the hydrostatic and non-hydrostatic mapping functions (here Global Mapping Functions (GMF), Böhm et al. 2006), mf_G is the gradient mapping function,

G_{ns} and G_{ew} represent the north-south (NS) and east-west (EW) delay gradient contributions, respectively, a is the azimuth of the line of sight of the individual observation. The ZHD accounts for about 90% of the total tropospheric delay and the ZWD for the remaining about 10% (Davis et al. 1985). The ZHD can be accurately calculated using empirical models such as the Saastamoinen (1973) model involving in-situ air pressure information. However, it is difficult to model ZWD with enough accuracy due to its very low mixing ratio with the dry atmospheric constituents, its high temporal variability and its dependence on atmospheric weather conditions that may significantly differ from the in-situ meteorological conditions. Thus, ZWD is usually estimated as an unknown parameter in the adjustment together with the other parameters.

In the real-time PPP ZTD/PWV processing, first the precise satellite orbits and clocks are determined using data of a global GPS+GLONASS ground tracking network. Similar to the procedure of the IGS ultra-rapid orbits, the real-time orbit is predicted (six hour prediction) based on the orbits determined in a batch-processing mode. Then, with fixed satellite orbits and station coordinates, satellite clocks are estimated and updated epoch-wise due to their short-term fluctuations (Zhang et al. 2011). With these real-time orbit/clock corrections and precise station coordinates, the estimated parameter vector \mathbf{X} can be described as,

$$\mathbf{X} = \left(ZWD \cdot G_{ns} \cdot G_{ew} \cdot dt \cdot B_P^{R_k-G} \cdot \mathbf{N} \right)^T \quad (6)$$

A sequential least square filter is employed to estimate the unknown parameters in real-time processing. The ZWD and the gradients G_{ns} and G_{ew} are modeled as random walk processes. The noise intensity of the quantity of most interest, ZWD, is about 5-10 mm/ \sqrt{h} . The receiver clock bias dt is modeled as white noise process and estimated epoch-wise.

The code biases $B_p^{R_k-G}$ are estimated as constant over time. As mentioned above, the phase biases will be absorbed by the phase ambiguities \mathbf{N} , and the ambiguity parameters are estimated as constant during each continuous arc. An elevation-dependent weighting strategy is applied as well.

ZWD derived from real-time PPP can be converted into PWV (Askne and Nordius 1987) by,

$$PWV = \Pi(T_m) \cdot ZWD \quad (7)$$

$$\Pi(T_m) = \frac{10^6}{\rho_w R_v \left(\frac{k_3}{T_m} + k_2' \right)} \quad (8)$$

where $\Pi(T_m)$ varies as a function of the weighted mean temperature of the atmosphere T_m (Bevis et al. 1992), $\rho_w = 999.97 \text{ kg m}^{-3}$ represents the density of liquid water, $R_v = 461.51 \text{ JK}^{-1} \text{ kg}^{-1}$ is the specific gas constant of water vapor, k_3 and k_2' denote atmospheric refractivity constants ($k_2' = 22.1 \pm 2.2 (\text{K hpa}^{-1})$, $k_3 = 373900 \pm 1200 (\text{K}^2 \text{ hpa}^{-1})$). To accurately calculate T_m , vertical profiles of water vapor and temperature are required (Davis et al. 1985):

$$T_m = \frac{\int \left(\frac{e}{T} \right) dz}{\int \left(\frac{e}{T^2} \right) dz} \approx \frac{\sum_{i=1}^N \left(\frac{e_i}{T_i} \right) \Delta z_i}{\sum_{i=1}^N \left(\frac{e_i}{T_i^2} \right) \Delta z_i} \quad (9)$$

where e denotes the partial pressure of water vapor, and T is the temperature. The information about the two variables can only be obtained from external meteorological resources for the PWV retrieving in this study.

One of the methods to derive T_m is presented by Bevis et al. (1992), where T_m is described as a linear function of surface temperature observations and vertical temperature

lapse rates. However, Wang et al. (2005) pointed out that this empirically calculated mean temperature tends to be less accurate, with a cold bias in the tropics and subtropics, and a warm bias in mid and high latitudes. This kind of defect of the Bevis model can be attributed to the fact that it only depends on radiosonde observations over the North American territory. In contrast, T_m interpolated from the global reanalysis of the ECMWF (European Centre for Medium-Range Weather Forecasts) can well represent the desired quantities at the locations of GNSS stations (Wang et al. 2005). Thus, in this study, T_m from ECMWF reanalysis ERA-Interim (http://apps.ecmwf.int/datasets/data/interim_land/) is adopted to perform the conversion from ZWD into PWV.

VLBI data

Various studies have illustrated that VLBI is capable of determining accurate tropospheric delays as well as water vapor content in the vicinity of the VLBI stations (Heinkelmann et al. 2007; Schuh and Böhm 2012). Since GNSS and VLBI observations are subject to the same type of errors in terms of the atmospheric effect, tropospheric parameter derived from VLBI provide an excellent basis for the comparison and validation of parameters retrieved by GNSS, which has been shown by many authors (Teke et al. 2011; Ning et al. 2012). In this study, VLBI data from the latest CONT campaign (CONT14, <http://ivs.nict.go.jp/mirror/program/cont14/>) are used to validate the real-time ZTD estimates derived from GLONASS and GPS. CONT14 is a special campaign of the International VLBI Service for Geodesy and Astrometry (IVS), aimed at acquiring state-of-the-art VLBI data over a time period of 15 days in order to demonstrate geodetic results of the highest accuracy

the current VLBI system is capable of. The CONT14 campaign was observed in the period 2014 May 6-20, with a network size of 17 globally distributed stations. Several stations from this network are co-located with the IGS GNSS stations mentioned above, which will be employed for the comparison and validation here.

For the analysis of VLBI observations acquired during CONT14, the GFZ version of the Vienna VLBI Software ([Böhm et al. 2012](#)), VieVS@GFZ, is used, where the unknown parameters are estimated in a classical least squares adjustment. The calculation of the theoretical delays follows the IERS Conventions 2010. The ZHD are modeled using Saastamoinen ([1973](#)) model with meteorological data from GPT2 ([Lagler et al. 2013](#)), in a consistent way compared to the a priori ZHD for the GNSS data processing. The estimated parameters included clock corrections, earth orientation parameters (EOP), ZWD, and horizontal gradients. The ZWD were parameterized as piece-wise linear functions with interval length of 1 hour and gradients are estimated with interval length of 6 hours. Comparable to the GNSS, the GMF are used as hydrostatic and wet mapping functions, and the elevation cut-off angle is set to 5° .

Radiosonde data

Radiosondes directly measure temperature, pressure, and humidity along their flight paths from the launch site upwards and communicate their records via a radio signal downlink. The radiosonde balloons are launched every 12 or 24 hours per day in most of the cases. As one of the most reliable in-situ measurement of water vapor ([Rocken et al. 1995](#); [Neill et al. 2001](#)), water vapor retrieved from the radiosonde is taken as another validation of the GLONASS- and GPS-derived PWV. For the comparison, all stations from the abovementioned

GPS/GLONASS observing network are employed, where nearby radiosonde launch sites (the distance is smaller than 50 km) are available. The radiosonde data profiles are provided by the National Ocean and Atmospheric Administration (NOAA, <http://www.esrl.noaa.gov/raobs/>).

In radiosonde data analysis, temperature, pressure, and humidity from the radiosonde profiles are utilized to retrieve PWV (Bevis et al. 1992). If linear water vapor density variation for each vertical level of the radiosonde profile is assumed, the PWV is calculated as,

$$PWV = \frac{1}{\rho_w} \sum (h_{i+1} - h_i) \cdot (\rho_v^{i+1} + \rho_v^i) / 2 \quad (10)$$

$$\rho_v = \frac{e_w}{R_v \cdot T} \quad (11)$$

where the variable ρ_v denotes the density of water vapor, ρ_w is the density of liquid water, the super- and subscripts $i+1$ and i denote the top and bottom of each layer for height and water vapor density, T is the temperature, e_w is the partial pressure of water vapor, which can be acquired from humidity and temperature, and $R_v = 461.525 J \cdot K^{-1} \cdot kg^{-1}$ is the specific gas constant of water vapor.

ZTD comparisons between GLONASS and GPS solutions

In order to assess the performance of the GLONASS-derived real-time ZTD/PWV, and evaluate the contribution of adding GLONASS to GPS for ZTD/PWV retrieval, we processed about 80 stations from the IGS network for the first half of the year 2014, where the GLONASS and GPS observations are simultaneously available. GLONASS-only, GPS-only,

and GPS/GLONASS combined PPP solutions are carried out to generate the ZTD/PWV estimates. All the data are processed in real-time PPP mode with 30 s sampling interval following the description in [GNSS data collection and processing](#) section.

Figure 2 exemplarily shows the ZTD time series of two stations during the first half of the year 2014: AUTO (30.39°N, 97.73°W), Austin, TX, USA, and WARK (36.43°S, 174.66°E), Warkworth, New Zealand. It can be seen that, in general, the GLONASS ZTD agree quite well with the GPS ZTD derived from real-time PPP. Compared to the GPS-only solution, neither an increased number of outliers nor a larger noise appears in the GLONASS-only solution. The scatter plot of ZTD between the two solutions at station AUTO is displayed in Figure 3. The correlation coefficient is 0.99, implying very high correlation between the GLONASS ZTD and GPS ZTD.

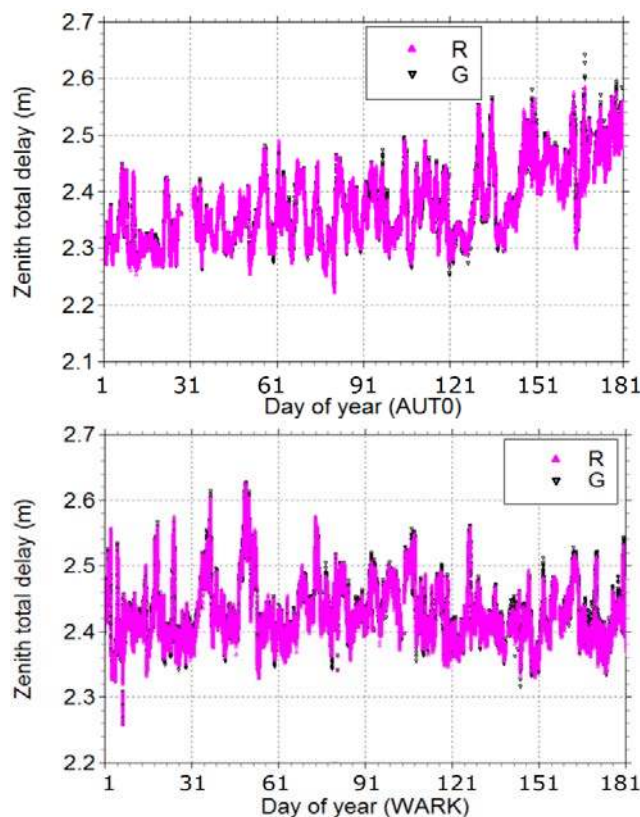


Figure 2 ZTD derived from GPS-only (“G”) and GLONASS-only (“R”) real-time PPP

solutions at stations AUTO (top) and WARK (bottom) for DOY (day of year) 001-181, 2014.

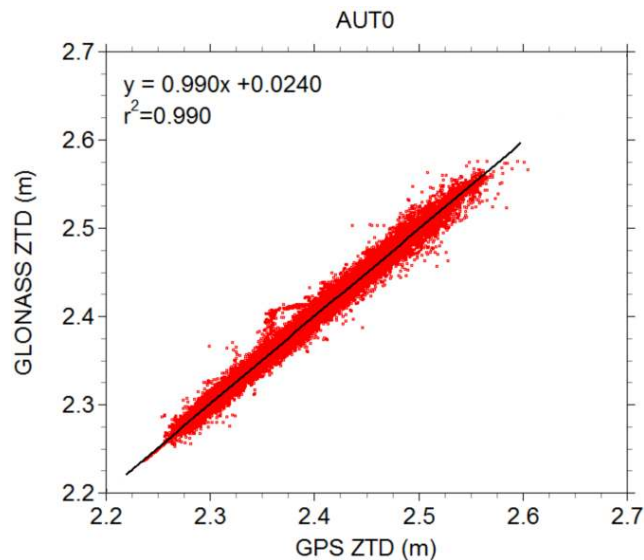


Figure 3 Scatter plot of ZTD between the GLONASS-only and GPS-only solutions at station AUTO.

Figure 4 presents the corresponding distributions of ZTD differences between GLONASS-only and GPS-only solutions at the abovementioned stations AUTO and WARK, during the same time period. The sign convention is GLONASS - GPS. It can be noticed that, the ZTD differences range from -15 mm to +15 mm on average, and the histogram is close to the normal distribution. The root mean square (RMS) of the ZTD differences at the two stations is 6.0 mm and 6.7 mm, respectively, showing an agreement at the level of several millimeters. No obvious systematic biases can be seen between the GLONASS- and GPS-only solutions. The mean values of the differences between GLONASS- and GPS-derived ZTD are 0.4 mm and -0.5 mm for the two stations, respectively.

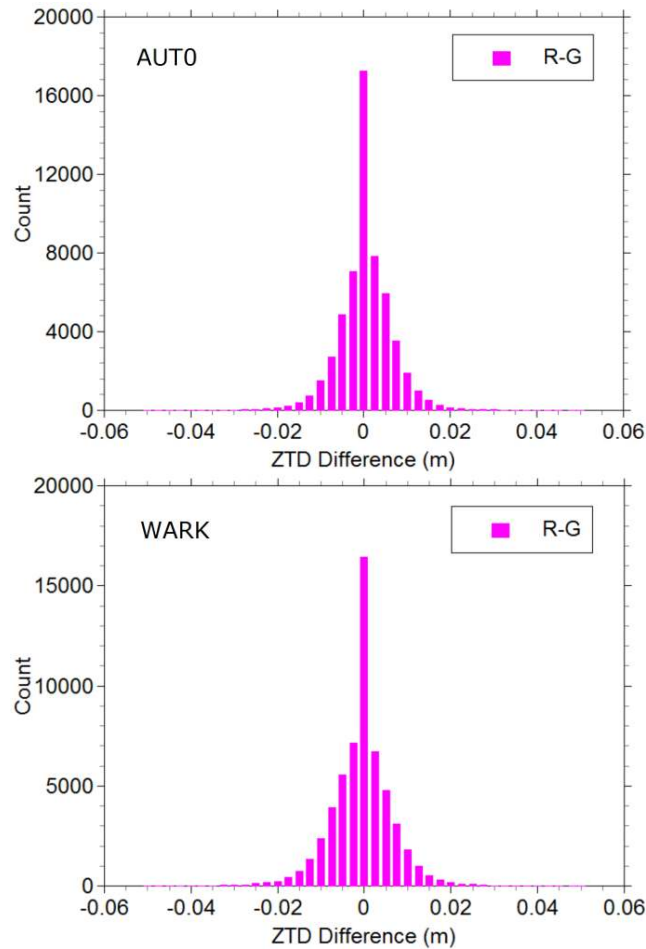


Figure 4 Distribution of ZTD differences between GLONASS-only and GPS-only solutions derived from real-time PPP at stations AUTO (top) and WARK (bottom) for DOY 001-180, 2014

In Figure 5, the statistical results of ZTD differences between GLONASS-only and GPS-only solutions are shown for about 80 stations. The RMS values of the ZTD differences are about 5-13 mm (which equals 0.8-2.0 mm in PWV), and the mean values of the differences are at the level of a few millimeters (smaller than 1 mm in PWV). In general, the ZTD estimates from GLONASS-only and GPS-only solutions show better agreement for high-latitude stations than for low-latitude stations. There are no significant geographical patterns of systematic biases of ZTD estimates between GLONASS and GPS solutions. This agreement

implies that the real-time ZTD/PWV estimates derived from GLONASS observations can significantly contribute to weather nowcasting, with a comparable accuracy as the GPS-only solution.

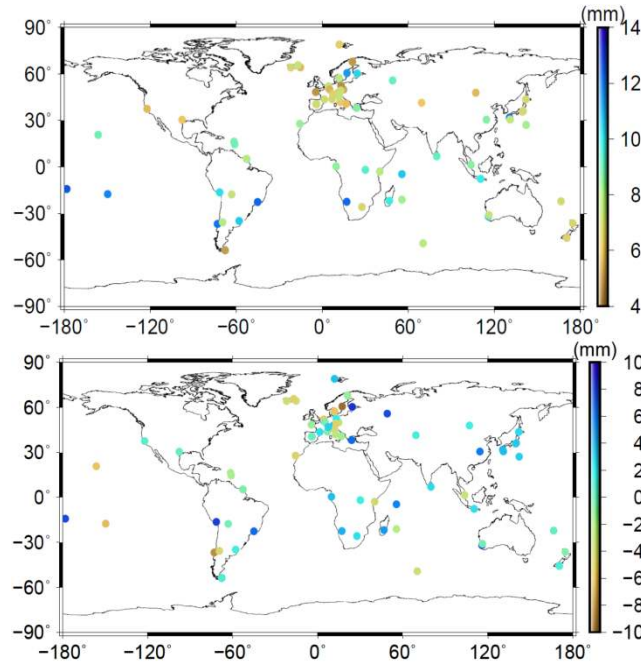


Figure 5 Geographical distribution of station-specific RMS values (top) and mean biases (bottom) of ZTD differences between GLONASS-only and GPS-only solutions determined with real-time PPP (DOY 001-181, 2014).

In order to further assess the internal consistency of the GLONASS ZTD, data from the co-located GNSS stations are taken into account. Figure 6 shows the ZTD comparison between the two co-located stations WTZR and WTZZ (height difference about 0.1 m) operated at Bad Koetzing, Germany, for the GLONASS-only and the GPS-only solutions. It can be noticed from Figure 6a that the ZTD derived from the GLONASS-only solutions for the two stations displays a rather good agreement. The RMS of the ZTD difference is about 6.2 mm and the mean value is about 0.3 mm. These results are comparable to those for the GPS-only solutions (shown in Figure 6b), where the RMS and mean value of the ZTD difference are about 6.6 mm and 0.4 mm, respectively. It proves that the ZTD derived from

GLONASS show good internal consistency comparable to the GPS.

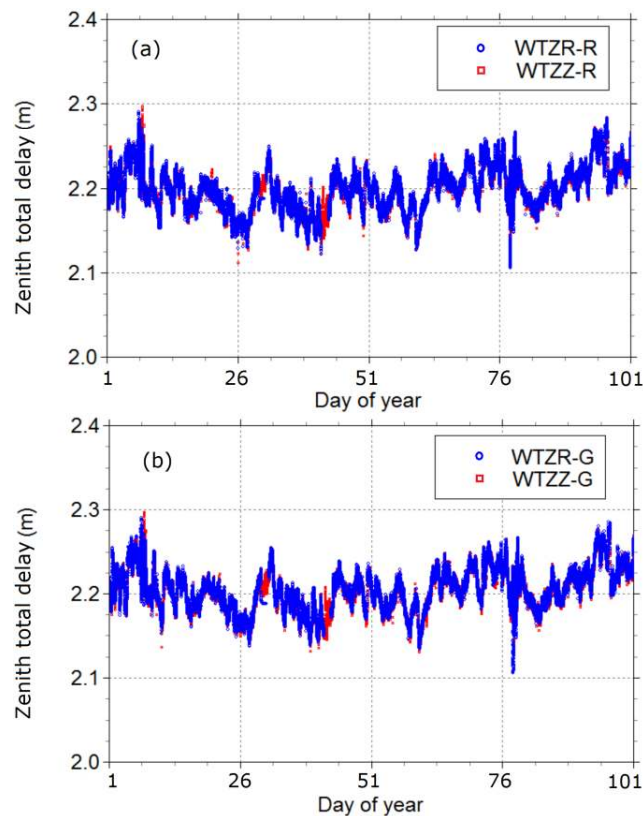


Figure 6 ZTD comparison for the co-located GNSS stations WTZR and WTZZ (Bad Koetzing, Germany) for DOY 001-101, 2014: (a) ZTD from the GLONASS-only solutions, (b) ZTD from the GPS-only solutions.

Validations with VLBI and radiosondes

For the purpose of inter-technique validation, the GNSS ZTD series retrieved from real-time PPP processing are compared with that from co-located VLBI stations. VLBI data from the CONT14 campaign are processed for ZTD derivation following the description in [VLBI data](#) section. To avoid additional interpolation, only ZTD estimates at common epochs of each ZTD series are taken into account for the comparison. The ZTD biases caused by the height difference between the phase center of GNSS antennas and the reference point of VLBI

telescopes are corrected by using the ‘troposphere ties’ method presented by Teke et al. (2011). Figure 7 shows the ZTD comparisons of GPS-only, GLONASS-only, GPS/GLONASS combined and VLBI solutions at the stations WARK (co-located with the VLBI station WARK12M) and TSK2 (co-located with the VLBI station TSUKUB32).

It can be noticed that the ZTD of the GLONASS-only, GPS-only and GPS/GLONASS combined solutions all reveal good agreement with the VLBI ZTD. The ZTD estimates of the GLONASS-only solution are comparable with that of the GPS-only solution. The RMS of GLONASS-only solution is 11.5 mm and 8.0 mm, and the RMS of GPS-only solution is 11.2 mm and 7.7 mm, respectively, at the two stations WARK and TSK2. Furthermore, the ZTD differences are the smallest for the GPS/GLONASS combined solution, where the RMS are 10.6 mm and 7.1 mm and the mean values of the differences are -1.0 mm and 0.36 mm for the two stations.

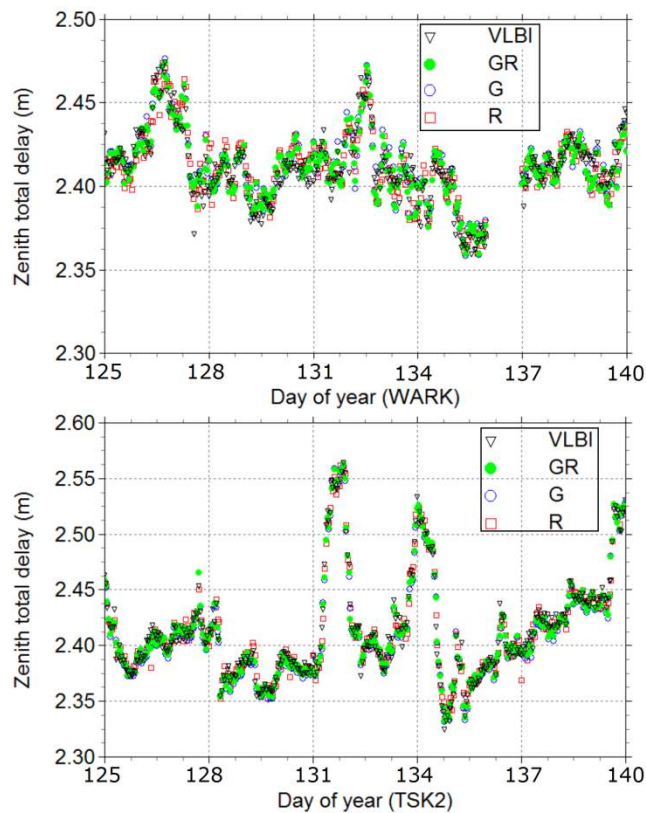


Figure 7 ZTD derived from GPS-only, GLONASS-only, GPS/GLONASS combined (“GR”)

and VLBI solutions at co-located stations WARK/WARK12M (top) and TSK2/TSUKUB32 (bottom) for DOY 125-140, 2014, i.e. 2014 May 6-20 (the CONT14 campaign).

In Figure 8, the RMS values of the ZTD differences for the GLONASS-only, GPS-only and GPS/GLONASS combined solutions with respect to the VLBI solutions are given for five co-located GNSS/VLBI stations (HARB, NYA2, TSK2, WARK, and WTZR). It can be seen that the RMS of ZTD differences between GLONASS- and GPS-only solutions vs. VLBI are both around several millimeters (about 1 cm), while the RMS of the combined solution shows the smallest values for all the stations. The RMS of the ZTD differences is 6.1-11.5 mm for the GLONASS-only solution, 6.0-11.2 mm for the GPS-only solution, and 5.1-10.6 mm for the GPS/GLONASS combined solution.

This confirms the abovementioned conclusion that the real-time ZTD retrieved from GLONASS-only solution are accurate and can be assimilated into NWP models and applied in weather nowcasting. Moreover, the GPS/GLONASS combined solutions can improve the accuracy and robustness of retrieved real-time ZTD/PWV compared to the single-system solutions.

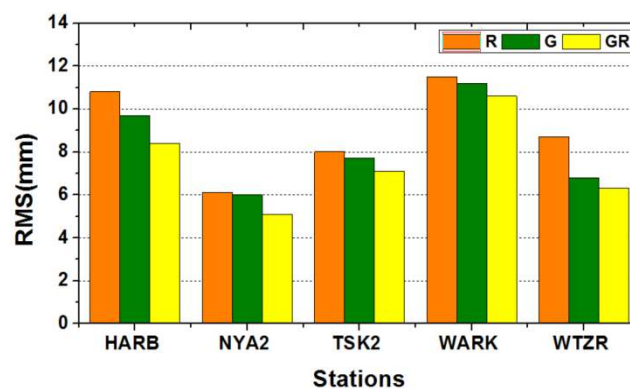


Figure 8 RMS of the ZTD for the GLONASS-only, GPS-only, and GPS/GLONASS

combined solutions with respect to the VLBI solution during CONT14.

The validation of the PWV values derived from the real-time GNSS PPP analysis versus radiosondes PWV is also performed. Figure 9 shows the PWV results retrieved from GPS/GLONASS combined real-time PPP solution and nearby radiosonde solution at station STFU (37.42°N, 122.17°E), Palo Alto, CA, USA. The radiosonde-retrieved PWV is sampled every 12 or 24 hours, while the temporal resolution of real-time PWV solutions derived from GNSS is 30 s. Only PWV values at the common epochs are considered for the comparison. It can be noticed that the PWV retrieved from the GPS/GLONASS combined solution agrees well with the radiosonde PWV with differences at the level of few millimeters, and the RMS of the PWV differences between the two solutions is about 1.5 mm.

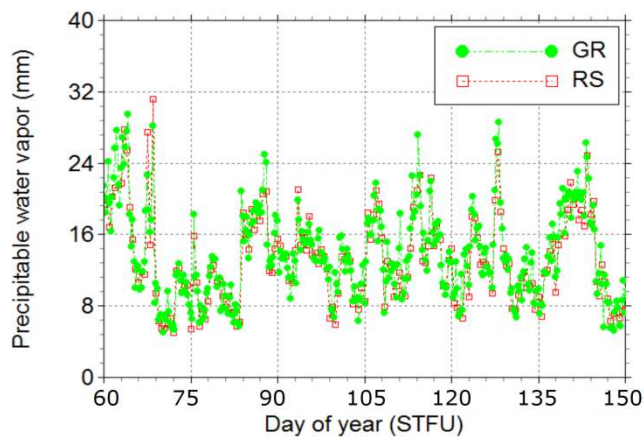


Figure 9 PWV derived from the GPS/GLONASS combined real-time PPP and radiosonde (“RS”) solutions at station STFU, Palo Alto, CA, USA, during days of year (DOY) 60-150 of 2014.

Figure 10 gives the RMS of the PWV differences for the GLONASS-only, GPS-only, and

GPS/GLONASS combined solutions with respect to the radiosonde solutions at 12 globally distributed GNSS stations, where nearby radiosonde launch sites (distance smaller than 50 km) are available. The RMS of the two single-system and the combined solutions all stay within 3 mm, which is the threshold accuracy of PWV for assimilation into NWP models (De Haan 2006). The GLONASS-only solution even shows a slightly smaller RMS than the GPS-only solution in some cases (e.g. HOFN and MAS1). The RMS for the combined solution shows the smallest values for almost all the stations. The RMS of the PWV differences is 1.8-2.6 mm for the GLONASS-only solution, 1.6-2.4 mm for the GPS-only solution, and 1.5-2.3 mm for the GPS/GLONASS combined solution. This indicates a potential benefit for real-time PWV retrieval from GLONASS if applied in time-critical meteorological fields such as NWP nowcasting and severe weather event monitoring compared to GPS. Furthermore, compared to the single-system solutions, higher accuracy and robustness can be achieved with the combination of GLONASS and GPS data in real-time PPP processing for meteorological applications.

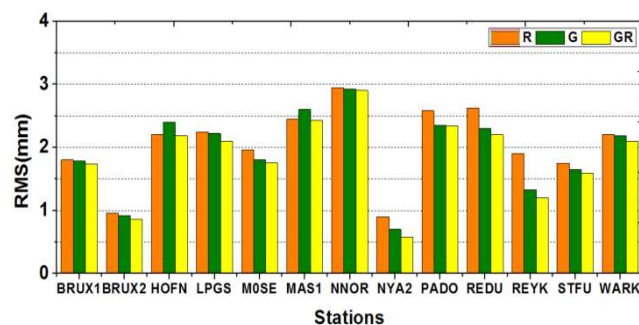


Figure 10 RMS of the PWV differences for the GLONASS-only, GPS-only, and GPS/GLONASS combined solutions with respect to the radiosonde solutions. BRUX1 and BRUX2 are two radiosonde stations close to the GNSS station BRUX.

Summary, conclusions and discussions

We have developed a real-time ZTD/PWV processing with GLONASS observations only, as well as with the combination of GPS and GLONASS observations. GLONASS and GPS data of about 80 stations from IGS network for the first half of the year 2014 were processed using the real-time PPP technique. The performance of the real-time ZTD/PWV estimates derived from GLONASS were analyzed and assessed, and the contribution of combining GLONASS to the stand-alone GPS solution for ZTD/PWV retrieval has been investigated as well.

The results show that the GLONASS ZTD derived from real-time PPP solution agree well with the GPS ZTD. The RMS values of the ZTD differences between the two solutions range from 5 mm to 13 mm (what equals a PWV of 0.8-2 mm), and the mean values of the differences are at the level of a few millimeters (usually < 1 mm in PWV). Furthermore, the GLONASS ZTD at co-located GNSS stations also show good internal consistency comparable to the ones obtained with GPS.

For validation, ZTD estimates of the two single-system solutions, GLONASS- and GPS-only, show good agreement with the ZTD derived from VLBI. The ZTD differences between the GLONASS-only solution and the VLBI solution are comparable to the ones of the GPS-only solution. The RMS of ZTD differences between the GLONASS-only solution and the VLBI solution are around several millimeters (6.1-11.5 mm), and 6.0-11.2 mm for the GPS-only solution. The ZTD differences are the smallest for the GPS/GLONASS combined solution, for which the RMS ranges from 5.1 to 10.6 mm. For the validation with radiosondes, the PWV from the GPS/GLONASS combined solution agree quite well with the PWV

derived from radiosondes, with differences at the level of a few millimeters, RMS of 1.5-2.3 mm (< 3 mm). The PWV of the single-system solutions, GLONASS-only and GPS-only, show a good agreement with PWV from radiosondes. The RMS of the PWV differences is 1.8-2.6 mm for the GLONASS-only solution, and 1.6-2.4 mm for the GPS-only solution. Therefore, we can conclude that GLONASS can contribute to real-time meteorological applications with comparable accuracy to that of GPS, and more robust and accurate ZTD/PWV estimates can be obtained, if the GLONASS observations are added to the GPS observations in real-time PPP mode.

In future our studies will focus on comparisons and validations involving other techniques, such as water vapor radiometer (WVR) and numerical weather models (NWM), and on a larger number of globally distributed GNSS stations and over a longer time span. Furthermore, the application of real-time PWV retrieval from GLONASS-only or GPS/GLONASS combined solutions in monitoring or nowcasting actual weather events, such as heavy rainfall or other extreme events, will be investigated as well.

Acknowledgements. We acknowledge IGS for providing the GPS and GLONASS data, IVS for providing the VLBI data, and NOAA for the online provision of radiosonde data. One of the authors (C. Lu) is supported by the China Scholarship Council, which is gratefully acknowledged.

References

- Askne, J. and H. Nordius (1987), Estimation of tropospheric delay for microwaves from surface weather data, *Radio Science* 22, 379-386.
- Böhm, J., A. Niell, P. Tregoning, and H. Schuh (2006), Global Mapping Function (GMF): A new empirical mapping function based on numerical weather model data, *Geophys. Res. Lett.* 33, L07304, doi:10.1029/2005GL025546.
- Böhm, J., S. Böhm, T. Nilsson, A. Pany, L. Plank, H. Spicakova, K. Teke, and H. Schuh (2012), The new Vienna VLBI Software VieVS, *Geodesy for Planet Earth*. In: *Proceedings of the 2009 IAG symposium, Buenos Aires, International Association of Geodesy Symposia Series*, vol 136, 1007-1011.
- Bevis, M., S. Businger, T. Herring, C. Rocken, R. Anthes, and R. Ware (1992), GPS meteorology: remote sensing of atmospheric water vapor using GPS, *J Geophys Res* 97:15787-15801.
- Bruyninx, C. (2007), Comparing GPS-only with GPS + GLONASS positioning in a regional permanent GNSS network, *GPS Solut* 11(2):97-106.
- Caissy, M., L. Agrotis, G. Weber, M. Hernandez-Pajares, and U. Hugentobler (2012), The International GNSS Real-Time Service, *GPS World*, 23 (6): 52-58.
- Cai, C. and Y. Gao (2013), Modeling and assessment of combined GPS/GLONASS precise point positioning, *GPS Solut* 17(2):223-236.
- Chen, G. and T. Herring (1997), Effects of atmospheric azimuthal asymmetry on the analysis of space geodetic data, *J Geophys Res* 102(B9):20489-20502. doi:10.1029/97JB01739.
- Dach, R. S. Schaer, and U. Hugentobler (2006), Combined multi-system GNSS analysis for

time and frequency transfer, Proc. Eur. Freq. Time Forum, 2006, 530-537.

De Haan, S. (2006), National/regional operational procedures of GPS water vapour networks and agreed international procedures, Rep.WMO/TD-No, 1340, 20, KNMI, Netherlands.

Dow, J., R. Neilan, and C. Rizos (2009), The International GNSS Service in a changing landscape of Global Navigation Satellite Systems, J. Geod. 83(3):191-198, doi: 10.1007/s00190-008-0300-3.

Davis, J., T. Herring, I. Shapiro, A. Rogers, and G. Elgered (1985), Geodesy by radio interferometry: Effects of atmospheric modeling errors on estimates of baseline length, Radio Sci. 20(6), 1593-1607, doi:10.1029/RS020i006p01593.

Dach, R., R. Schmid, M. Schmitz, D. Thaller, S. Schaer, S. Lutz, P. Steigenberger, G. Wübbena, and G. Beutler (2011), Improved antenna phase center models for GLONASS, GPS Solut 15(1): 49-65.

Dousa, J. (2010), Precise near real-time GNSS analyses at geodetic observatory Pecny-precise orbit determination and water vapour monitoring, Acta Geodyn. Geomater. 7 (157), 7-17.

Dousa, J. and P. Vaclavovic (2014), Real-time zenith tropospheric delays in support of numerical weather prediction applications, Adv Space Res, 53(9), 1347-1358.

Elgered, G., H. Plag, H. van der Marel, S. Barlag, and J. Nash (eds.) (2005), COST 716: Exploitation of ground-based GPS for climate and numerical weather prediction applications, Final Report, European Community, EUR 21639, ISBN 92-898-0012-7.

Gendt, G., G. Dick, C. Reigber, M. Tomassini, Y. Liu, and M. Ramatschi (2004), Near real-time GPS water vapor monitoring for numerical weather prediction in Germany, J. Meteorol. Soc. Jpn. 82, 361- 370.

- Gutman, S., R. Sahn, G. Benjamin, E. Schwartz, L. Holub, Q. Stewart, and L. Smith (2004), Rapid retrieval and assimilation of ground based GPS-Met observations at the NOAA forecast systems laboratory: impact on weather forecasts, *J Meteorol Soc Jpn* 82:351-360.
- Haan, S., S. Barlag, H. Baltink, and F. Debie (2004), Synergetic use of GPS water vapor and meteosat images for synoptic weather forecasting, *J. Appl. Met.* 43, 514-518.
- Heinkelmann, R., J. Böhm, H. Schuh, S. Bolotin, G. Engelhardt, D. MacMillan, M. Negusini, E. Skurikhina, V. Tesmer, and O. Titov (2007), Combination of long time-series of troposphere zenith delays observed by VLBI, *J. Geod.* 81, 6-8, 483-501.
- Kouba, J. (2009), A Guide to Using International GNSS Service (IGS) Products, <http://igsb.jpl.nasa.gov/igsb/resource/pubs/UsingIGSProductsVer21.pdf>.
- Lagler, K., M. Schindelegger, J. Boehm, H. Krásná, and T. Nilsson (2013), GPT2: Empirical slant delay model for radio space geodetic techniques, *Geophys. Res. Lett.* 40, 1069-1073, doi:10.1002/grl.50288.
- Li, X., G. Dick, M. Ge, S. Heise, J. Wickert, and M. Bender (2014), Real-time GPS sensing of atmospheric water vapor: precise point positioning with orbit, clock and phase delay corrections, *Geophys. Res. Lett.* 41(10), 3615-3621.
- Li, X., X. Zhang, X. Ren, M. Fritsche, J. Wickert, and H. Schuh (2015), Precise positioning with current multi-constellation Global Navigation Satellite Systems: GPS, GLONASS, Galileo and BeiDou, *Sci Rep.* 5, 8328.
- Melgard, T., E. Vigen, K. Jong, D. Lapucha, H. Visser, and O. Oerpen (2009), G2—the first real-time GPS and GLONASS precise orbit and clockservice. *Proc. ION GNSS 2009*, Institute of Navigation, Savannah, GA, 22-25September, 1885-1891.

- Niell, A., A. Coster, F. Solheim, V. Mendes, P. Toor, R. Langley, and C. Upham (2001), Comparison of measurements of atmospheric wet delay by radiosonde, water vapor radiometer, GPS, and VLBI, *J Atmos Oceanic Technol* 18:830-850.
- Nilsson, T. and G. Elgered (2008), Long-term trends in the atmospheric water vapor content estimated from ground-based GPS data, *J. Geophys. Res.* 113:D19101, doi: 10.1029/2008JD010110.
- Ning, T., R. Haas, G. Elgered, and U. Willén (2012), Multi-technique comparisons of 10 years of wet delay estimates on the west coast of Sweden, *J. Geod.* 86 (7), 565-575, doi:10.1007/s00190-011-0527-2.
- Piriz, R., D. Calle, A. Mozo, P. Navarro, D. Rodriguez, and G. Tobias (2009), Orbits and clocks for GLONASS precise point positioning. *Proc. ION-GNSS-2009*, Institute of Navigation, Savannah, Georgia, Sept 22-25, 2415-2424.
- Rocken, C., T. Van Hove, and R. Ware (1997), Near real-time sensing of atmospheric water vapor, *Geophys. Res. Lett.* 24, 3221-3224.
- Schuh, H. and D. Behrend (2012), VLBI: A fascinating technique for geodesy and astrometry, *J Geodyn* 61, 68-80, DOI 10.1016/j.jog.2012.07.007.
- Shi, J., C. Xu, J. Guo, and Y. Gao (2015), Real-Time GPS Precise Point Positioning-Based Precipitable Water Vapor Estimation for Rainfall Monitoring and Forecasting, *Geoscience and Remote Sensing, IEEE Transactions on*, 53 (6), no.6, 3452-3459, doi: 10.1109/TGRS.2014.2377041.
- Saastamoinen, J. (1973), Contributions to the theory of atmospheric refraction - Part II.

Refraction corrections in satellite geodesy,

Bull.Géod.47(1),13-34,doi:10.1007/BF02522083.

Teke, K., J. Boehm, T. Nilsson, H. Schuh, P. Steigenberger, R. Dach, R. Heinkelmann, P.

Willis, R. Haas, S. Garcia-Espada, T. Hobiger, R. Ichikawa, and S. Shimizu (2011),

Multi-technique comparison of troposphere zenith delays and gradients during CONT08,

J. Geod. 85:395-413, doi:10.1007/s00190-010-0434-y.

Wang, J., L. Zhang, and A. Dai (2005), Global estimates of water-vapor-weighted mean

temperature of the atmosphere for GPS applications, J. Geophys. Res. 110, D21101,

doi:10.1029/2005JD006215.

Wanninger, L. (2011), Carrier-phase inter-frequency biases of GLONASS receivers, J Geod.

doi:10.1007/s00190-011-0502-y.

Yuan, Y., K. Zhang, W. Rohm, S. Choy, R. Norman, and C. Wang (2014), Real-time retrieval

of precipitable water vapor from GPS precise point positioning, J. Geophys. Res. Atmos.

119, 10,044-10,057.

Zhang, X., X. Li, and F. Guo (2011), Satellite clock estimation at 1 Hz for real-time

kinematic PPP applications, GPS Solut 15(4):315-324. doi:10.1007/s10291-010-0191-7.

Zumberge, J., M. Heflin, D. Jefferson, M. Watkins, and F. Webb (1997), Precise point

positioning for the efficient and robust analysis of GPS data from large networks, J.

Geophys. Res. 102(B3):5005-5017.

Author Biographies (50-60 words per author).



Cuixian Lu is currently working toward the Ph.D. degree at GFZ. Her current research focuses mainly involve space geodetic techniques for troposphere.



Dr. Xingxing Li is a scientist at GFZ. His current research focuses mainly involve GNSS precise data processing and its application for geosciences.



Dr. Maorong Ge is a senior scientist at GFZ. His research interests are GNSS algorithms and software development.



Dr. Robert Heinkelmann is a scientist at GFZ. His research interests are Very Long Baseline Interferometry (VLBI) technique and its applications.



Dr. Tobias Nilsson is a scientist at GFZ. His research interests are VLBI technique and its applications.



Benedikt Soja is currently working toward the Ph.D. degree at GFZ. His current research focuses mainly involve Kalman Filtering for VLBI processing.



Dr. Galina Dick is a senior scientist at GFZ. His research interests are GNSS meteorology.



Prof. Harald Schuh is currently the Director of Dept. 1 “Geodesy and Remote Sensing” at GFZ. His research interests are VLBI technique and its applications.